AD-A128 680 RADAR RESONANCE REFLECTION FROM SETS OF PLANE DIELECTRIC LAYERS(U) COAST GUARD WASHINGTON DC OFFICE OF RESEARCH AND DEVELOPMENT P D JACKINSL ET AL. MAY 83 USCG-D-14-83 1/1

UNCLASSIFIED F/G 17/9 NL

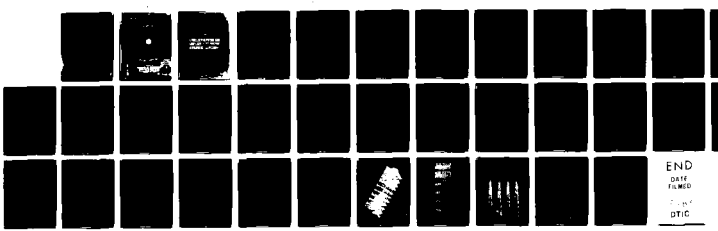

END

DATE FILMED

DTIC

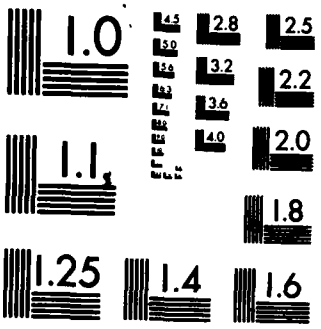

MICROCOPY RESOLUTION TEST CHART
NATIONAL BUREAU OF STANDARDS-1963-A

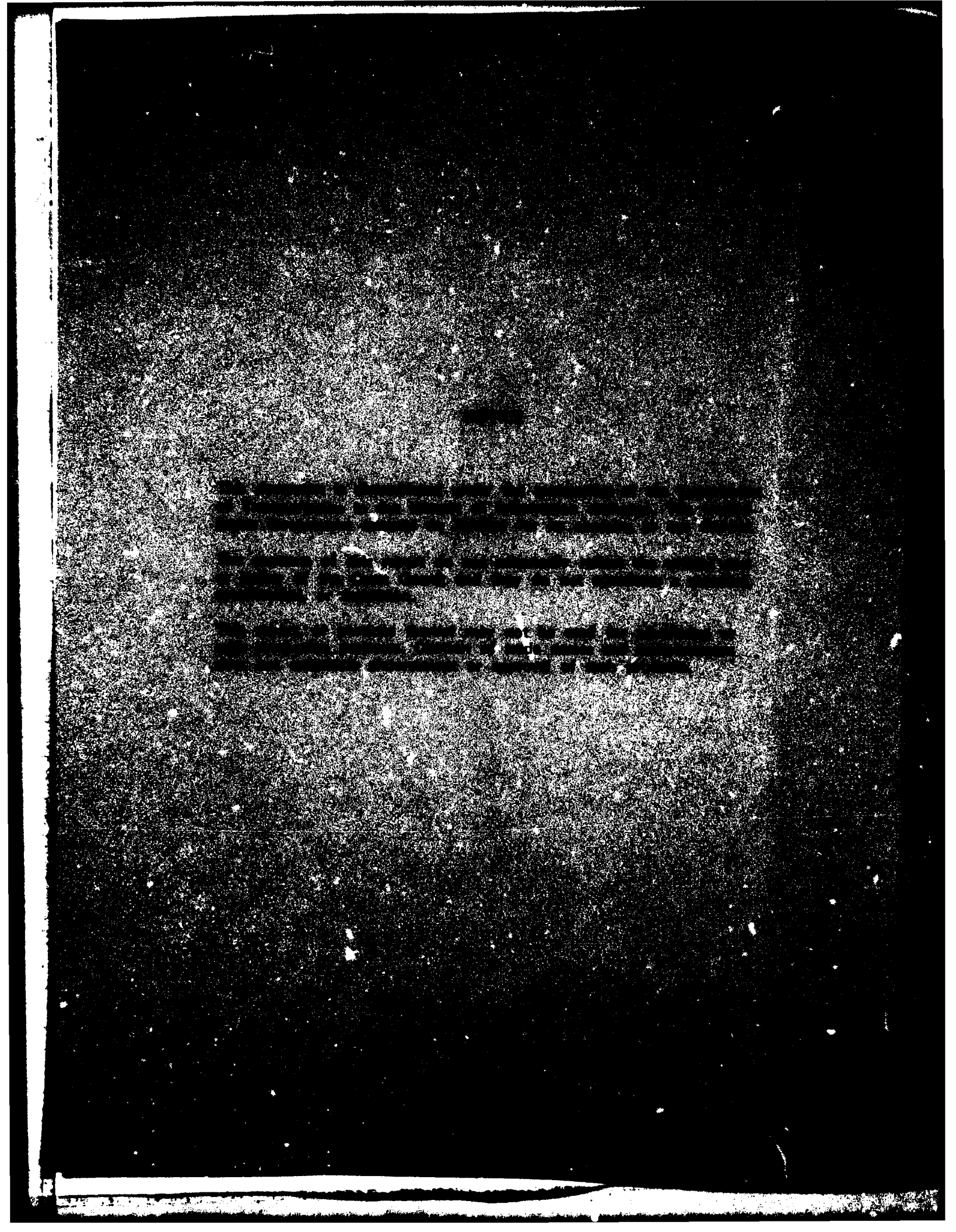

Technical Report Documentation Page

1. Report No.	2. Government Accession No.	3. Recipient's Catalog No.
CG-D-14-83	AD-A128680	

4. Title and subtitle
Radar Resonance Reflection from Sets of Plane Dielectric Layers

5. Report Date
May 1983

6. Performing Organization Code
DOT/USCG

7. Author(s)
P.D. Jackins and G.C. Gaunaurd

8. Performing Organization Report No.

9. Performing Organization Name and Address
Naval Surface Weapons Center
White Oak, Silver Spring, MD 20910

10. Work Unit No. (TRAIS)
814108.32.2

11. Contract or Grant No.

12. Sponsoring Agency Name and Address
U.S. Coast Guard
Office of Research and Development
Washington, DC 20593

13. Type of Report and Period Covered

14. Sponsoring Agency Code
G-DMT-4/54

15. Supplementary Notes

16. Abstract

The prediction of the Resonance Scattering Theory (RST) for the reflection coefficient from a set of two contiguous plane dielectric layers separating two semi-infinite dissimilar non-conducting media, is constructed and compared to the exact classical model solution. The comparison serves to: a) show the accuracy and simplicity of the RST prediction, and b) to underline the usefulness of the RST to produce simple physical interpretations of generally complex phenomena. The analysis provides a systematic method for detecting the presence of a dielectric layer under another one covering it (possibly the situation caused by an oil spill in ice-covered Arctic regions), by certain modulation effects present in the "response surface" of the returned echoes. This method also identifies the material composition of the lower or hidden layer in the bilaminar configuration. The process disentangles which resonance feature present in the radar reflection coefficient is caused by which of the two interacting layers. RST, therefore, solves the inverse scattering problem for the composition and thickness not only of the top visible (ice) layer, but also of the substance (oil) hidden under that upper layer.

17. Key Words
Radar
Oilspill Detection
Reflection Coefficient
Electromagnetic Profiling
Resonance Scattering Theory

18. Distribution Statement
Document is available to the public through the National Technical Information Service, Springfield, Virginia, 22161.

19. Security Classif. (of this report)	20. Security Classif. (of this page)	21. No. of Pages	22. Price
Unclassified	Unclassified	29	

Form DOT F 1700.7 (8-72) Reproduction of completed page authorized

METRIC CONVERSION FACTORS

Approximate Conversions to Metric Measures

Symbol	When You Know	Multiply by	To Find	Symbol
		LENGTH		
in	inches	*2.5	centimeters	cm
ft	feet	30	centimeters	cm
yd	yards	0.9	meters	m
mi	miles	1.6	kilometers	km
		AREA		
in^2	square inches	6.5	square centimeters	cm^2
ft^2	square feet	0.09	square meters	m^2
yd^2	square yards	0.8	square meters	m^2
mi^2	square miles	2.6	square kilometers	km^2
	acres	0.4	hectares	ha
		MASS (weight)		
oz	ounces	28	grams	g
lb	pounds	0.45	kilograms	kg
	short tons (2000 lb)	0.9	tonnes	t
		VOLUME		
tsp	teaspoons	5	milliliters	ml
Tbsp	tablespoons	15	milliliters	ml
fl oz	fluid ounces	30	milliliters	ml
c	cups	0.24	liters	l
pt	pints	0.47	liters	l
qt	quarts	0.95	liters	l
gal	gallons	3.8	liters	l
ft^3	cubic feet	0.03	cubic meters	m^3
yd^3	cubic yards	0.76	cubic meters	m^3
		TEMPERATURE (exact)		
°F	Fahrenheit temperature	5/9 (after subtracting 32)	Celsius temperature	°C

*1 in = 2.54 (exactly). For other exact conversions and more detailed tables, see NBS Misc. Publ. 286, Units of Weights and Measures, Price $2.25, SD Catalog No. C13.10:286.

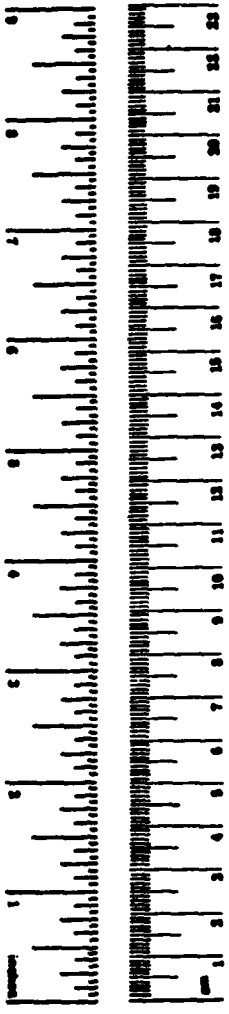

Approximate Conversions from Metric Measures

Symbol	When You Know	Multiply by	To Find	Symbol
		LENGTH		
mm	millimeters	0.04	inches	in
cm	centimeters	0.4	inches	in
m	meters	3.3	feet	ft
m	meters	1.1	yards	yd
km	kilometers	0.6	miles	mi
		AREA		
cm^2	square centimeters	0.16	square inches	in^2
m^2	square meters	1.2	square yards	yd^2
km^2	square kilometers	0.4	square miles	mi^2
ha	hectares (10,000 m^2)	2.5	acres	
		MASS (weight)		
g	grams	0.035	ounces	oz
kg	kilograms	2.2	pounds	lb
t	tonnes (1000 kg)	1.1	short tons	
		VOLUME		
ml	milliliters	0.03	fluid ounces	fl oz
l	liters	2.1	pints	pt
l	liters	1.06	quarts	qt
l	liters	0.26	gallons	gal
m^3	cubic meters	35	cubic feet	ft^3
m^3	cubic meters	1.3	cubic yards	yd^3
		TEMPERATURE (exact)		
°C	Celsius temperature	9/5 (then add 32)	Fahrenheit temperature	°F

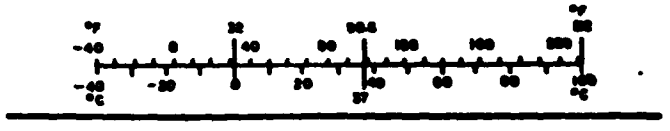

TABLE OF CONTENTS

LIST OF TABLES

LIST OF FIGURES

RADAR RESONANCE REFLECTION FROM SETS OF PLANE DIELECTRIC LAYERS

P. D. Jackins and G. C. Gaunaurd
Naval Surface Weapons Center
White Oak, Silver Spring, MD 20910

ABSTRACT

The prediction of the Resonance Scattering Theory (RST) for the reflection coefficient from a set of two contiguous plane dielectric layers separating two semi-infinite dissimilar non-conducting media, is constructed and compared to the exact classical model solution. The comparison serves to: a) show the accuracy and simplicity of the RST-prediction, and b) to underline the usefulness of the RST to produce simple physical interpretations of generally complex phenomena. The analysis provides a systematic method for detecting the presence of a dielectric layer under another one covering it (possibly the situation caused by an oil spill in ice-covered Arctic regions), by certain modulation effects present in the "response surface" of the returned echoes. This method also identifies the material composition of the lower or hidden layer in the bilaminar configuration. The process disentangles which resonance feature present in the radar reflection coefficient is caused by which of the two interacting layers. This, therefore, solves the inverse scattering problem for the composition and thickness not only of the top visible (ice) layer, but also of the substance (oil) hidden under that upper layer.

INTRODUCTION

For many years wave reflection and transmission through penetrable layered media has been a well plowed field of research where solutions usually have been given in terms of reflection and transmission coefficients. These coefficients describe the energy fraction returned by, or transmitted through, the (possibly layered) scatterer (1-7). While such solutions are exact, they are so cumbersome for systems of two or more plane interacting layers that they hardly ever permit a quick understanding of the physics behind

the results. A novel analytical approach denoted the Resonance Scattering Theory (RST) (8) has been recently developed at NSWC. This method has been applied to many probelms dealing with the scattering of (acoustic, electromagnetic and elastic) waves by penetrable objects, mostly of simple shapes (8). While the results generated by means of the RST are mostly approximations, their simplicity and accuracy permits a greater insight and deeper understanding of the physical mechanisms involved in their generation than was ever before possible.

In general, under the dissecting knife of the RST, each of the partial waves (or normal modes) making up the total scattered field by a target can be subdivided into two contributions. The first one, denoted the "background," represents the wave-field returned by an otherwise identical but impenetrable scatterer. The second portion of the scattered wave-field represents, and is caused by, the resonances of the internal penetrable material making up the scatterer (8). The splitting described above also holds for the reflection coefficient from plane layers where the "backgrounds" are usually constants. The RST was recently applied to the problem of sound transmission/reflection through/by a liquid layer embedded within one fluid (9), and later when the liquid layer separates two dissimilar fluids (10). In electromagnetism the method was first conceived and developed for the spherical geometry (11), and presently for sets of plane, dielectric, interacting layers.

I. THE CLASSICAL MODEL

We are particularly concerned here with the detection and possible material characterization of thin petroleum (oil) layers lying beneath a relatively thick overlayer of ice using radar echoes. We will model here, however, a general situation consisting of two interacting layers (ice and oil) separating an upper (air) from a lower (water) medium while (radar) electromagnetic waves are incident on the bilaminar system from the upper (air) side. (See Figure 1.) We exploit here the fact that both substances have different dielectric constants and different thicknesses, which will excite certain characteristic "resonance features" in the returned radar echoes. These features can be made manifest and much more understandable under the light of the RST.

We assume that the bilaminar system is composed of two ideally bonded layers with the upper one (ice) thicker than the lower one (oil). Following the approach of Brekhovskikh (6) the oil-water interface is chosen as the origin of the coordinate system, as shown in Figure 1, while the water (medium 1) and the air (medium 4) are considered to be semi-infinite in the $\pm z$ directions. Media 2 and 3, of thicknesses d_2 and d_3, are the oil and the ice, respectively, and we further assume that $d_2 < d_3$. The incident electromagnetic wave is assumed to emanate from a distant source in medium 4 and it is polarized with the electric vector $\vec{E}$ parallel to the media

interfaces. Maxwell's equations in Gaussian units are

$$\vec{\nabla} \times \vec{H} = \frac{4\pi\sigma}{c_0} \vec{E} + \frac{\varepsilon}{c_0} \frac{\partial \vec{E}}{\partial t} \quad , \quad \vec{\nabla} \cdot \vec{E} = 0 \qquad (1)$$

$$\vec{\nabla} \times \vec{H} = -\frac{\mu}{c_0} \frac{\partial \vec{H}}{\partial t} \quad , \quad \vec{\nabla} \cdot \vec{H} = 0$$

where ε is the dielectric constant, c_0 is the speed of light in vaccuum, and μ, σ are the permeability, conductivity of the medium supporting the wave, respectively. For plane monochromatic waves with time-dependence $e^{-i\omega t}$, Maxwell's equations reduce to:

$$\vec{\nabla} \times \vec{H} = -\frac{i\omega\varepsilon'}{c_0} \vec{E} \quad , \quad \vec{\nabla} \times \vec{E} = \frac{i\omega\mu}{c_0} \vec{H} \qquad (2)$$

where

$$\varepsilon' = \varepsilon + i \frac{4\pi\sigma}{\omega} \quad . \qquad (3)$$

In general, air, fresh water, oil, and fresh water ice are sufficiently poor conductors so that $\sigma \approx 0$. We note that salt water and salt water ice are relatively better conductors, and thus, corrections are needed in such instances. The (vector) Helmholtz equation for $\vec{E}$ is found by taking the curl of the second of Eqs. (2), and using the first of Eqs. (2) to eliminate the curl of $\vec{H}$. The result is

$$(\nabla^2 + k^2) \vec{E} = 0 \qquad (4)$$

where

$$k = \frac{\omega}{c_0} \sqrt{\varepsilon\mu} \approx \frac{\omega}{c_0} \sqrt{\varepsilon} \qquad (5)$$

Here, $\omega = 2\pi f$ is the angular frequency of the incident wave, and c_0 the speed of light in vacuum (i.e., $c_0 = 3 \times 10^{10}$ cm/sec).

Since there is a physical discontinuity at each media interface, several boundary conditions must be satisfied. It is thus required that between the jth and the $j+1$ media,

$$(E_j)\tan = (E_j+1)\tan$$
$$(H_j)\tan = (H_j+1)\tan \qquad (6)$$

This is a statement of continuity of the tangential components for the electric and magnetic fields across the various interfaces.

The electric field in medium (4) is given by

$$E_y = \left\{A_4 \exp\left[-i\, k_4(z - z_3)\cos\theta_4\right] + B_4\left[\exp\ ik_4(z - z_3)\cos\theta_4\right]\right\}\exp\left[ik_4 z \sin\theta_4\right]\hat{j} \qquad (7)$$

where A_4 and B_4 are the amplitude coefficients of the incidence and reflected waves, respectively, $z_3 = d_2 + d_3$ is the location of the interface separating media (3) and (4), while θ_4 is the incidence angle. The tangential component of the magnetic field in medium (4) is given, using Eq. (2), by

$$H_{4x} = \frac{1}{z_4}\left\{A_4 \exp\left[-ik_4(z-z_3)\cos\theta_4\right] - B_4 \exp\left[ik_4\,(z-z_3)\cos\theta_4\right]\right\} \cdot \cdot \exp\left[ik_4 z \sin\theta_4\right] \qquad (8)$$

where

$$z_4 = \frac{\sqrt{\mu_4\varepsilon_4}}{\cos\theta_4} \simeq \frac{1}{\sqrt{\varepsilon_4}\cos\theta_4} \qquad (9)$$

is the field impedance defined as the ratio of the tangential component of the electric field to the tangential component of the magnetic field. Similar expressions are obtained for the electric and magnetic fields in the other three media. In medium (1) one has $B_1 = 0$ because there is no reflected wave. The connecting bond between phase-relationships on either side of a boundary is provided by Snell's law, which is,

$$k_4 \sin\theta_4 = k_i \sin\theta_i \qquad \text{for } i = 1, 2, 3 \qquad (10)$$

where

$$k_i = \frac{\omega}{v_i} = \frac{\omega}{c_0}\sqrt{\epsilon_i} \qquad ($$

Three sets of equations involving the coefficients Aj and Bj can be obtained using the boundary conditions, Eqs. (6), at the interfaces. [i. e., $z=0$, $z=d_2$, and $z=d_2 + d_3$] In particular, on the boundary separating the 2nd and 3rd medium, the boundary conditions to be satisfied (Eqs. (6)) are,

$$A_2 \exp(-ik_2 d_2 \cos\theta_2) + B_2 \exp(ik_2 d_2 \cos\theta_2) = A_3 + B_3 \qquad (12)$$

$$A_2 \exp(-ik_2 d_2 \cos\theta_2) - B_2 \exp(ik_2 d_2 \cos\theta_2) = \frac{z_2}{z_3}(A_3 - B_3)$$

Inspection of Figure 1 shows that the reflection coefficient R is given by the ratio

$$R = \frac{B_4}{A_4} . \qquad (13)$$

Similar expressions can be obtained for the continuity conditions at the two other interfaces which then can be used to determine A_4 and B_4 in terms of A_1. After all the reductions, the reflection coefficient of the bilaminar system under study is

$$R = \frac{A^- \cos\delta_2\cos\delta_3 - B^- \sin\delta_2\sin\delta_3 - i\left[C^- \sin\delta_2\cos\delta_3 + D^- \cos\delta_2\sin\delta_3\right]}{A^+ \cos\delta_2\cos\delta_3 - B^+ \sin\delta_2\sin\delta_3 - i\left[C^+ \sin\delta_2\cos\delta_3 + D^+ \cos\delta_2\sin\delta_3\right]} \qquad (14)$$

where

$$
\begin{aligned}
A^{\pm} &= z_2 z_3 (z_1 \pm z_4) \\
B^{\pm} &= z_1 z_3^2 \pm z_2^2 z_4 \\
C^{\pm} &= z_3 (z_2^2 \pm z_1 z_4) \\
D^{\pm} &= z_2 (z_3^2 \pm z_1 z_4)
\end{aligned}
\tag{15}
$$

and

$$
\begin{aligned}
\delta_2 &= \frac{2\pi}{c_0} (fd_3) \frac{1}{\alpha} \sqrt{\varepsilon_2} \quad \sqrt{1 - \frac{\varepsilon_4}{\varepsilon_2} \sin^2\theta_4} \\
\delta_3 &= \frac{2\pi}{c_0} (fd_3) \quad \sqrt{\varepsilon_3} \sqrt{1 - \frac{\varepsilon_4}{\varepsilon_3} \sin^2\theta_4}
\end{aligned}
\tag{16}
$$

and α is the thickness ratio $\alpha = d_3/d_2 > 1$. In the case where $\vec{E}$ is parallel to the air-ice interface, the impedances are

$$
z_j = 1/\left[\sqrt{\varepsilon_j} \cos\theta_j\right] \qquad (j = 1, 2, 3, 4)
\tag{17}
$$

and also

$$
z_j = \cos\theta_j/\sqrt{\varepsilon_j} \qquad (j = 1, 2, 3, 4)
$$

for the case where $\vec{E}$ is parallel to the plane of incidance.

The numerical values used in this analysis for the dielectric constants are as follows:

Air: $\varepsilon_4 = 1$; Ice: $\varepsilon_3 = 3.2$

Oil: $\varepsilon_2 = 2$; Water: $\varepsilon_1 = 81$ (18)

In the limiting case where $d_2 \to 0$ (and $\delta_2 \to 0$), the reflection coefficient reduces to that of a single layer of thickness d separating two different media, viz,

$$R = \frac{z_3(z_1 - z_4)\cos\delta_3 - i\left[z_3^2 - z_1 z_4\right]\sin\delta_3}{z_3(z_1 + z_4)\cos\delta_3 - i\left[z_3^2 + z_1 z_4\right]\sin\delta_3} \tag{19}$$

This same result is also obtained from Eq. (14) when media (2) and (3) are the same [i. e., $z_2 = z_3, \varepsilon_2 = \varepsilon_3$]. For completeness, we also give the transmission coefficient T for the double layer system

$$T = \frac{2z_1 z_2 z_3/\cos\delta_2\cos\delta_3}{A^+ - B^+\tan\delta_2\tan\delta_3 - i\left[C^+\tan\delta_2 + D^+\tan\delta_3\right]} = \frac{A_1}{A_4} \tag{20}$$

which for one layer (i. e., $d_2 \to 0$ $\delta_2 \to 0$) reduces to

$$T = \frac{2z_1 z_3}{z_3(z_1 + z_4)\cos\delta_3 - i\left[z_3^2 + z_1 z_4\right]\sin\delta_3} \tag{21}$$

Equations (14) [or (20)] and (19) [or (21)] are exact solutions for the reflection coefficient [or the transmission coefficient] for a two-layer and one-layer dielectric slab, respectively, separating two semi-infinite non-conductive media.

The square of the magnitude of R can be expressed as

$$|R|^2 = \frac{z_3^2(z_1 - z_4)^2\cos^2\delta_3 + (z_3^2 - z_1 z_4)^2\sin^2\delta_3}{z_3^2(z_1 + z_4)^2\cos^2\delta_3 + (z_3^2 + z_1 z_4)^2\sin^2\delta_3} \tag{22}$$

for a single layer, and

$$|R|^2 = \frac{\left[A^-\cos\delta_2\cos\delta_3 - B^-\sin\delta_2\sin\delta_3\right]^2 + \left[C^-\sin\delta_2\cos\delta_3 + D^-\cos\delta_2\sin\delta_3\right]^2}{\left[A^+\cos\delta_2\cos\delta_3 - B^+\sin\delta_2\sin\delta_3\right]^2 + \left[C^+\sin\delta_2\cos\delta_3 - D^+\cos\delta_2\sin\delta_3\right]^2} \tag{23}$$

for the bilaminar configuration.

Plots of target cross-sections or of reflection coefficients $|R|^2$ as functions of frequency (or frequency-thickness products) and of another variable such as angle of incidence θ_4 have been referred to as "response surfaces" in the past (12). The response surface for a single ($d_2 \to 0$) layer (parallel $\vec{E}$ polarization) is shown in Figure 2 for frequency-thickness products ranging from 0 to 900 MHz-meters, and incidence angles θ_4 from 0^0 (normal) to 90^0 (grazing). This response surface exhibits a series of peaks and valleys which are seen to be evenly spaced in planes of constant incidence angles, but unevenly spaced in planes of constant fd_3 products. The minimum values of $|R|^2$ correspond to values for which the real part of the denominator of R vanishes. They approximate the resonance frequencies of the layer of thickness d_3. For the case of a single layer system, these resonances occur for phase delays δ's which are odd multiples of $\pi/2$. For normal incidence cases, this corresponds to plate thickness which are proportional to an odd number of quarter-wavelengths. These eigenfrequencies are the natural resonances for the unloaded plate.

For the bilaminar system, the resonances occur at values of the frequency thickness products fd_3 and of the incidence angle θ_4 for which

$$A^+ \cos\delta_2 \cos\delta_3 = B^+ \sin\delta_2 \sin\delta_3 \ . \qquad (24)$$

For fixed incidence angles, this characteristic equation determines the frequency-thickness resonances $(fd_3)_i$ of the bilaminar system (i=1, 2,...n). Note that Eq. (24) represents the vanishing of the real part of the denominator of Eq. (14).

Figs. 3 and 4 exhibit the response surface for the bilaminar system, for various polarizations, ice-to-oil thickness ratios, and in various frequency regimes. The six parts of Fig. 3 are all produced for incidence angles θ_4 in the range $0 \leq \theta_4 \leq 90^0$ and for the frequency-thickness products in the range $0 \leq fd_3 \leq 900$MHz-meter. The upper-most plot in Fig. 3 is for perpendicular polarization, (see Fig. 1) a case of little interest in this analysis, while the other five plots are all for the case of parallel (i. e., $\vec{E}_{||}$) polarization. The second plot of Fig. 3 corresponds to the case of a single layer with parallel polarization. The following plots (third to sixth from the top) are for decreasing values of the parameter α as follows: third, for α=500; fourth, α=100; fifth, α=10; and sixth, α=5. These correspond to increasingly thicker layers of oil (d_2) relative to a fixed layer of ice (d_3). The last one, for example, corresponds to an ice layer five times thicker than the oil layer. Figure 4 presents again the response surface, all for parallel polarization, but in the much larger range of frequency-thickness products going from 0 to 3 GigaHertz-meter. Highly inclined ridges appear in the response surface in the higher

frequency parts of the ranges. The top plot is for a single layer, or a double layer with $\alpha=\infty$. The second to fourth plots correspond to α values of $\alpha=50{,}000$, 500 and 5, respectively. These plots are all exact, no approximation having been introduced yet. Practical radars operate in the upper portions of these plots.

From Eq. (24) [or Eq. (19)], it follows that for a single layer (i. e., $\delta_2 \to 0$) the characteristic equation giving the resonances reduces to $\cos\delta_3=0$. Table 1 presents a listing of the first twenty roots of the bilaminar situation governed by Eq. (24). This table is constructed for the same thickness ratios considered in Fig. 4 which are $\alpha \equiv d_3/d_2$ = 50,000, 500, and 5 MHz-meter. Table 1 is constructed for the case of normal incidence $\theta_4=0^0$. Table 2 contains exactly the same information as in Table 1 but for an incidence angle of $\theta_4=30^0$. These entries correspond to the location of the minima in Fig. 4, but in the planes $\theta_4=0^0$ and 30^0, respectively.

II. MODEL FORMULATION IN TERMS OF THE RESONANCE SCATTERING THEORY

The RST formulation (8) first linearizes the terms appearing in the right hand side of Eq. (14) by means of a Taylor series truncated after its second term. We denote

$$F^{\pm}(fd_3) = A^{\pm}\cos\delta_2\cos\delta_3 - B^{\pm}\sin\delta_2\sin\delta_3 \tag{25}$$

then, the two-term Taylor series expansion about f_{on} is (for each n):

$$F^{\pm}(fd_3) = F^{\pm}(f_{on}d_3) + (f - f_{on})\, d_3 \frac{\partial F^{\pm}}{\partial(fd_3)}\Big]_{f=f_{on}} + \ldots\ldots \tag{26}$$

Here, f_{on} are the resonance frequencies, roots of Eq. (24) for constant incidence angle θ_4, or which are the same, they are the roots of

$$F^{+}(fd_3) = 0\,, \qquad (\text{for } f = f_{on}) \tag{27}$$

It is now clear that

$$F^{-}(f_{on}d_3) = A^{-}\cos\delta_{20}^{(n)}\cos\delta_{30}^{(n)} - B^{-}\sin\delta_{20}^{(n)}\sin\delta_{30}^{(n)}, \tag{28}$$

and

$$\frac{\partial F^{\pm}(f_{on}d_3)}{\partial(f_{on}d_3)} = -\left[\left(A^{\pm}\frac{\partial\delta_2}{\partial(fd_3)} + B^{\pm}\frac{\partial\delta_3}{\partial(fd_3)}\right)\Bigg|_{f=f_{on}} \sin\delta_{20}^{(n)}\cos\delta_{30}^{(n)} + \left(A^{\pm}\frac{\partial\delta_3}{\partial(fd_3)} + B^{\pm}\frac{\partial\delta_2}{\partial(fd_3)}\right)\Bigg|_{f=f_{on}} \sin\delta_{20}^{(n)}\cos\delta_{30}^{(n)}\right] \tag{29}$$

and the derivatives are found from Eqs. (16) to be:

$$\frac{\partial\delta_2}{\partial(fd_3)} = \frac{2\pi}{c_0}\,\frac{1}{\alpha}\,\sqrt{\varepsilon_2}\,\left(1 - \frac{\varepsilon_4}{\varepsilon_2}\sin^2\theta_4\right)^{\frac{1}{2}} \tag{30}$$

and

$$\frac{\partial\delta_3}{\partial(fd_3)} = \frac{2\pi}{c_0}\,\sqrt{\varepsilon_3}\,\left(1 - \frac{\varepsilon_4}{\varepsilon_3}\sin^2\theta_4\right)^{\frac{1}{2}}\,. \tag{31}$$

It is not hard to show that Eq. (14) can now be re-written as

$$R = \sum_{n=1}^{\infty} \frac{a + b(x - x_{on}) + i\, g(\Gamma_n/2)}{x - x_{on} + i\,(\Gamma_n/2)} \qquad (32)$$

where

$$\frac{\Gamma_n}{2} = -\frac{1}{\left[\frac{\partial F^+}{\partial x}\right]_{x_{on}}} \left[C^+ \sin\delta_{20}^{(n)} \cos\delta_{30}^{(n)} + D^+ \cos\delta_{20}^{(n)} \sin\delta_{30}^{(n)}\right] \qquad (33)$$

$$b = \left[\frac{\partial F^-}{\partial x} \Big/ \frac{\partial F^+}{\partial x}\right]_{x_{on}} \qquad (34)$$

$$g = \frac{C^- \sin\delta_{20}^{(n)} \cos\delta_{30}^{(n)} + D^- \cos\delta_{20}^{(n)} \sin\delta_{30}^{(n)}}{C^+ \sin\delta_{20}^{(n)} \cos\delta_{30}^{(n)} + D^+ \cos\delta_{20}^{(n)} \sin\delta_{30}^{(n)}} \qquad (35)$$

$$a = \frac{(A^- B^+ - A^+ B^-) \sin\delta_{20}^{(n)} \sin\delta_{30}^{(n)}}{A^+ \left[\frac{\partial F^+}{\partial x}\right]_{x_{on}}} \qquad (36)$$

and $x = f d_3$.

The form of the reflection coefficient in Eq. (32) exhibits the resonance character of the phenomenon. It was borrowed from nuclear scattering theory, where similar expressions a e associated with the names of Breit and Wigner (13), and it is now the central-type of expression for the RST-analysis of macroscopic scattering problems in electromagnetics, acoustics, and elastodynamics (8). The summation in Eq. (32) is merely symbolic, since the formula and the RST-approximation are only valid in the vicinity of the resonances, and the sum merely means that the neighborhoods of all the resonances must be accounted for. Each resonance x_{on} has a width Γ_n associated with the imaginary part of the simple denominator of Eq. (32).

In terms of the RST formalism, it follows from the above analysis, that the square of the modulus of R which is the quantity plotted in all the graphs, is given by

$$|R|^2 = \sum_{n=1}^{\infty} \frac{[a + b(x - x_{on})]^2 + g^2\Gamma_n^2/4}{(x - x_{on})^2 + \Gamma_n^2/4} \qquad (37)$$

for the bilaminar system. For the <u>single</u> layer, this expression reduces to

$$|R|^2 = \sum_{n} \frac{e^2(x - x_{on})^2 + f^2\gamma_n^2/4}{(x - x_{on})^2 + \gamma_n^2/4} \qquad (38)$$

where the x_{on} are now the roots of $\cos\delta_3 = 0$, rather than the roots of the characteristic equation (24), and where $a \to 0$ and

$$\begin{aligned} e &= (z_1 - z_4)/(z_1 + z_4) = A^-/A^+ \\ f &= (z_3^2 - z_1 z_4)/(z_3^2 + z_1 z_4) = D^-/D^+ \end{aligned} \qquad (39)$$

$$\tfrac{1}{2}\gamma_n = -\frac{D^+}{2A^+\frac{\partial\delta_3}{\partial x}} = -\frac{c_0}{2\pi\sqrt{\varepsilon_3}} \cdot \frac{(z_3^2 + z_1 z_4)}{z_3(z_1 + z_4)} \left[1 - \frac{\varepsilon_4}{\varepsilon_3}\sin^2\theta_4\right]^{-\frac{1}{2}}$$

and the layer of thickness d_2 (i. e., oil) has been removed since in this case $d_2 \to 0$. We have already shown in the acoustic case (14) how the casting of the expressions into the RST-forms can be made exact by means of Mittag-Leffler rather than Taylor series expansions, a point that will not be considered further here, since the approximate RST expressions developed here are adequately good and useful for our purposes. We note that the one-layer resonance relation in Eq. (38), obtained as a particular case of our more general Eq. (32), is the electromagnetic counterpart of an available acoustic relation (10) useful to study ocean bottom properties.

III. NUMERICAL CALCULATIONS AND DISCUSSION

The quantity $|R|^2$ is a scalar function of incidence angle θ_4 and frequency-thickness products fd_3. This quantity can be plotted three-dimensionally as we have shown before in Figs. 2, 3, and 4. It can also be plotted two-dimensionally versus one of the variables, keeping the other one fixed. For normal incidence (i. e., $\theta_4 = 0$), Fig. 5 shows the two-dimensional response curve (i. e., $|R|^2$ vs.

fd_3) in the range $0 \leq fd \leq 1{,}000$ megahertz-meters, first for a single layer of ice separating air from water (and for $E_{||}$ polarization), and later for a double layer of ice and oil with four levels of oil-thicknesses relative to the ice's. The relevant values of α in the bottom four graphs of Fig. 5 are $\alpha \equiv d_3/d_2 = 500$, 100, 25, 5, respectively. Two sets of curves are shown in these graphs, one in solid and the other in dashed lines. The solid lines represent the results of exact calculations using the (complicated) classical formulism that led to Eqs. (23), (15), and (16). It is quite difficult to interpret the physical phenomenon from these cumbersome expressions. The dashed lines represent the results of approximate calculations using the RST-formulism that led to Eqs. (33) - (37). It is quite evident from these plots that the RST-formulism generates each resonance "dip", one at a time, and that the agreement between dashed and solid curves near the tip of each minima (or dip) is nearly perfect, and only away from each resonance minima do differences become apparent between the two. In fact, the agreement betwen solid and dashed curves is near perfect down to the half-width of each resonance-dip, measured at half-minimum, and given by Eq. (33).

The RST-form in Eq. (37) or better in (32), is much clearer to understand and it represents the addition of contributions each emerging from a pole located at

$$x = x_{on} - i\,\Gamma_n/2 \qquad (40)$$

in the complex x-plane. We have expanded on this type of interpretation before (15) in similar instances. The real part of the pole-position gives the location of the resonance minimum in the $x = fd_3$ axis, and its imaginary part is its half-width. As shown in Fig. 5 as well as in Table 1, for a single layer the spacing between resonances, the magnitudes of $|R|^2$ at resonance, and the resonance half-widths are all constants. Further observation of Fig. 5 shows that when the ice layer is very thick compared to the oil layer (i. e., $\alpha = 500$), there is hardly any visible difference between the response curve for the bilaminar configuration and that of the single ice layer shown at the top of Fig. 5. The resonance locations, roots of Eq. (24), approach those of the single dielectric slab as $d_2 \to 0$. For ice-to-oil thickness ratios of 100 or less, the response curve of the bilaminar layer configuration starts to differ visibly from that of the single layer. The difference manifests itself in an upward slope of the response curve that culminates in the wavy undulations shown at the bottom of Fig. 5, where $\alpha = 5$. The pattern exhibited is similar to the modulation produced by the beating together of two sinusoidal waves of different frequencies. We repeat that all results displayed in Fig. 5 exhibit excellent agreement between the exact solution (solid lines) and the approximations inherent to the Resonance Scattering Theory (dashed lines). We remark that there is a minute difference between the exact resonances, at the minima points of the solid line graphs, and the RST (dashed) approximations, which is due to the presence of the

quantity "a" appearing in the numerator of Eq. (32), which is small for the case at hand. We also note that while the spacing between resonances and their widths were constants for the single-layer case, this no longer holds for the bilaminar configuration where a "cyclic" variation is now present.

IV. THE INVERSE SCATTERING PROBLEM

It is assumed that the electromagnetic properties of air and water, in this case ε_4, ε_1, are known. The solution of the inverse scattering problem then reduces to a determination of the paramters d_2, ε_2, d_3, ε_3 for the thicknesses and dielectric constants of the oil and ice layers. We will show that sufficient information can be extracted from a careful analysis of the response surfaces and curves presented in Figs. 2 through 6 to completely identify these parameters. The key to the solutionlies in an understanding of the characteristic Eq. (24) which determines the locations where resonances occur. The quantities A^+ and B^+ present in this equation depend on the dielectric constants of the four media involved in the reflection process, as well as on the initial incidence angle θ_4. For simplicity in the anlaysis we shall assume normal incidence although any oblique incidence could have been used just as well. The phase delays introduced by the two finite layers, δ_2 and δ_3, (c/o Eqs. 16) depend on the dielectric constant and thickness of the respective layer as well as on the frequency of the incident radiation. We note that if the thickness of the oil layer is small and the frequency is low, then δ_2 will have a small value. If it is further required that δ_3 not be small, then the characteristic Eq. (24) is approximated by

$$\cos\delta_3 = 0 \qquad (41)$$

which we saw was the resonance condition or characteristic equation for a single (upper) layer (of ice). Thus, at low frequencies, the bilaminar layer problem with a large ratio α of ice-to-oil thicknesses, behaves to first order like a single ice layer. However, as the frequency increases or as the oil layer thickness increases, the effects of the oil layer on the resulting response curves become more pronounced. There is a modulation effect visible in the response curves (c/o Fig. 5) and caused by the presence of the oil layer which was discussed in §III. We further note that in the bottom graph of Fig. 5, the first displayed resonance is very near in amplitude to that of the single ice layer given in the top graph of Fig. 5. As the frequency increases, the amplitude of the following resonances start to increase approaching a minimum which coincides with the value seen for a single oil layer in Fig. 6. How closely the resonances will approach those of the single oil layer is ultimately governed by Eq. (24). It, therefore, follows that the amplitude oscillations introduced by the modulation effect here described (c/o Fig. 5, bottom graph) are bounded by the extreme

values of the resonance amplitudes of the oil or the ice layers individually and the modulation is confined to occur in between them.

It can be seen from Eq. (32) that at any resonance

$$R = \sqrt{|R|^2} = \left[\frac{a^2}{(\Gamma_n/2)^2} + g^2\right]^{\frac{1}{2}} \tag{42}$$

where $\Gamma_n/2$, q, and a were given be Eqs. (33), (35) and (36), respectively. It is easily shown for resonances where either $\cos\delta_2$ or $\cos\delta_3$ is close to zero, that $a/(\Gamma_n/2)$ is negligibly small. By means of Eqs. (29) - (36) this ratio is

$$\frac{a}{(\Gamma_n/2)} = -\frac{(A^-B^+ - A^+B^-)\cos\delta_{20}^{(n)}\cos\delta_{30}^{(n)}}{B^+\,(C^+\sin\delta_{20}^{(n)}\sin\delta_{30}^{(n)} + D^+\cos\delta_{20}^{(n)}\sin\delta_{30}^{(n)})} \tag{43}$$

$$= \frac{A^+B^- - A^-B^+}{B^+} \cdot \frac{1}{[C^+\tan\delta_{20}^{(n)} + D^+\tan\delta_{30}^{(n)}]}$$

Thus, for large values of either $\tan\delta_{20}^{(n)}$ or $\tan\delta_{30}^{(n)}$, it follows that

$$|a/(\Gamma_n/2)| \leq [\tan\delta_{20}^{(n)}]^{-1} \text{ or } [\tan\delta_{30}^{(n)}]^{-1} \tag{44}$$

Hence, in the neighborhood of these resonances, the ratio $|2a/\Gamma_n|$ is negligible and any resonance amplitude is essentially given by

$$R \simeq g$$

which reduces to

$$R_0 = \frac{C^-}{C^+} \tag{45}$$

for an oil-type resonance provided that $\tan\delta_2 >> 1$, and to

$$R_1 = \frac{D^-}{D^+} \tag{46}$$

for an ice-type resonance provided that $\tan\delta_3 >> 1$.

For the specific problem considered here (i. e., ice and oil) the resonances with the smallest amplitudes (i. e., $|R|^2 \simeq 0.226$) are caused by the ice layer (see Fig. 5 top) while the resonances with the largest amplitudes (i. e., $|R|^2 \simeq 0.405$) are due to the oil layer (See Fig. 6). If the amplitudes of the ice and oil resonances, distinguished in this fashion, are represented by R_0 and R_i, respecitively, then it follows from Eqs. (45) and the expressions for $C\pm$ or $D\pm$ in Eqs. (15) that

$$z_2 = (z_1 z_4)^{\frac{1}{2}} \left(\frac{1 + R_0}{1 - R_0}\right)^{\frac{1}{2}} . \qquad (47)$$

The impedances z_1 and z_4 are known quantities, Eq. (9), while R_0 is determined from the calculated response surfaces of from patterns similar to those in Figs. 5 and 6 obtained from measurements. For normal incidence, Eq. (47) directly yields the dielectric constant of the hidden (oil) layer in the form

$$\varepsilon_2 = (z_1 z_4)^{-\frac{1}{2}} \left(\frac{1 - R_0}{1 + R_0}\right)^{\frac{1}{2}} . \qquad (48)$$

In a similar fashion, the dielectric constant for the upper (ice) layer is

$$\varepsilon_3 = (z_1 z_4)^{-\frac{1}{2}} \left(\frac{1 - R_i}{1 + R_i}\right)^{\frac{1}{2}} . \qquad (49)$$

In what follows we will assume these dielectric constants known and given by Eqs. (48), (49). Thus, all the constants $A\pm$, $B\pm$, $C\pm$, $D\pm$ appearing in Eq. (15) can be determined from selected resonance amplitudes in the reflection coefficient plots. The remaining still undetermined quantities are the thicknesses of the oil and the ice layers. This information can be extracted from the (half) widths of the resonances.

For the purposes of solving the inverse scattering problem, we note that the response surfaces and curves in Figs. 2-6 are all really found in practice as functions of frequency f, rather than frequency-thickness products fd_3. Figs. 2-6 have all been displayed versus x ($\equiv fd_3$) for convenience in the formulation and ease in the display, but with the understanding that f was the physical quantity varying along those axes since d_3 is not really known apriori. The difference between x and f is the constant scale factor d_3. If those response curves were displayed versus f, the amplitudes of the resonances would remain the same as in Figs. 2-6 but their width

would be changed by a factor of d_3. The widths Γ_n given in Eq. (33) in plots displayed versus x will now become widths Γ'_n in plots displayed versus f and they are given by

$$\frac{\Gamma'_n}{2} = - \frac{C^+ \sin\delta_{20}^{(n)} \cos\delta_{30}^{(n)} + D^+ \cos\delta_{20}^{(n)} \sin\delta_{30}^{(n)}}{d_3 \left[\frac{\partial F^+}{\partial x}\right]_{x_{on}}} \tag{50}$$

a value which differs from that in Eq. (33) by a scale factor d_3 now present in the denominator. It is clear that

$$d_3 \frac{\partial F^+}{\partial x} = \frac{\partial F^+}{\partial f}$$

and that

$$\left(\frac{\partial F^+}{\partial x}\right)_{x_{on}} = - \frac{2\pi}{c_0} \left\{\left[A^+ \sqrt{\varepsilon_2}\,\alpha^{-1} + B^+ \sqrt{\varepsilon_3}\right] \sin\delta_{20}^{(n)} \cos\delta_{30}^{(n)} + \left[A^+ \sqrt{\varepsilon_3} + B^+ \sqrt{\varepsilon_2}\,\alpha^{-1}\right] \cos\delta_{20} \sin\delta_{30}\right\} . \tag{51}$$

For an oil-type resonance, for which $\tan\delta_2 >> 1$, Eq. (50) gives the approximate result

$$\frac{\Gamma'_{n0}}{2} = \frac{C^+}{\frac{2\pi}{c_0} d_3 \left[A^+ \sqrt{\varepsilon_2}\,\alpha^{-1} + B^+ \sqrt{\varepsilon_3}\right]} , \tag{52}$$

and for an ice-type resonance, for which $\tan\delta_3 >> 1$,

$$\frac{\Gamma'_{ni}}{2} = \frac{D^+}{\frac{2\pi}{c_0} d_3 \left[A^+ \sqrt{\varepsilon_3} + B^+ \sqrt{\varepsilon_2}\,\alpha^{-1}\right]} .$$

Dividing these two equations one by the other and solving the result for α^{-1} ($\equiv d_2/d_3$) yields,

$$\alpha^{-1} = \left(\frac{\varepsilon_3}{\varepsilon_2}\right)^{\frac{1}{2}} \frac{A^+S - B^+}{A^+ - SB^+} \tag{54}$$

where

$$S = \frac{C^+}{D^+} \frac{\Gamma'_{ni}}{\Gamma'_{no}} \quad . \tag{55}$$

Once α^{-1} is known, either Eq. (52) or (54) can be used to determine d_2 and d_3. These thicknesses come out to be

$$d_2 = \frac{c_0}{\pi\sqrt{\varepsilon_2}} \frac{1}{A^{+2}-B^{+2}} \left[\frac{A^+C^+}{\Gamma'_{no}} - \frac{B^+D^+}{\Gamma'_{ni}}\right] \tag{56a}$$

$$d_3 = \frac{c_0}{\pi\sqrt{\varepsilon_2}} \frac{1}{B^{+2}-A^{+2}} \left[\frac{B^+C^+}{\Gamma'_{no}} - \frac{A^+D^+}{\Gamma'_{ni}}\right] \tag{56b}$$

which are expressed here in terms of measured widths Γ'_{no}, Γ'_{ni} and of quanitites such as A^+, B^+, C^+, D^+, ε_2, ε_3, all determined earlier. All the material and geometrical parameters required to completely solve the inverse scattering problem have been determined from the radar reflections.

would be changed by a factor of d_3. The widths Γ_n given in Eq. (33) in plots displayed versus x will now become widths Γ'_n in plots displayed versus f and they are given by

$$\frac{\Gamma'_n}{2} = - \frac{C^+ \sin\delta_{20}^{(n)} \cos\delta_{30}^{(n)} + D^+ \cos\delta_{20}^{(n)} \sin\delta_{30}^{(n)}}{d_3 \left[\frac{\partial F^+}{\partial x}\right]_{x_{on}}} \tag{50}$$

a value which differs from that in Eq. (33) by a scale factor d_3 now present in the denominator. It is clear that

$$d_3 \frac{\partial F^+}{\partial x} = \frac{\partial F^+}{\partial f}$$

and that

$$\left(\frac{\partial F^+}{\partial x}\right)_{x_{on}} = - \frac{2\pi}{c_0} \left\{\left[A^+ \sqrt{\varepsilon_2}\, \alpha^{-1} + B^+ \sqrt{\varepsilon_3}\right] \sin\delta_{20}^{(n)} \cos\delta_{30}^{(n)} + \left[A^+ \sqrt{\varepsilon_3} + B^+ \sqrt{\varepsilon_2}\, \alpha^{-1}\right] \cos\delta_{20} \sin\delta_{30}\right\} . \tag{51}$$

For an oil-type resonance, for which $\tan\delta_2 >> 1$, Eq. (50) gives the approximate result

$$\frac{\Gamma'_{n0}}{2} = \frac{C^+}{\frac{2\pi}{c_0} d_3 \left[A^+ \sqrt{\varepsilon_2}\, \alpha^{-1} + B^+ \sqrt{\varepsilon_3}\right]} , \tag{52}$$

and for an ice-type resonance, for which $\tan\delta_3 >> 1$,

$$\frac{\Gamma'_{ni}}{2} = \frac{D^+}{\frac{2\pi}{c_0} d_3 \left[A^+ \sqrt{\varepsilon_3} + B^+ \sqrt{\varepsilon_2}\, \alpha^{-1}\right]} .$$

Dividing these two equations one by the other and solving the result for α^{-1} ($\equiv d_2/d_3$) yields,

$$\alpha^{-1} = \left(\frac{\varepsilon_3}{\varepsilon_2}\right)^{\frac{1}{2}} \frac{A^+S - B^+}{A^+ - SB^+} \tag{54}$$

where

$$S = \frac{C^+}{D^+} \frac{\Gamma'_{ni}}{\Gamma'_{no}} \quad . \tag{55}$$

Once α^{-1} is known, either Eq. (52) or (54) can be used to determine d_2 and d_3. These thicknesses come out to be

$$d_2 = \frac{c_0}{\pi\sqrt{\varepsilon_2}} \frac{1}{A^{+2}-B^{+2}} \left[\frac{A^+C^+}{\Gamma'_{no}} - \frac{B^+D^+}{\Gamma'_{ni}}\right] \tag{56a}$$

$$d_3 = \frac{c_0}{\pi\sqrt{\varepsilon_2}} \frac{1}{B^{+2}-A^{+2}} \left[\frac{B^+C^+}{\Gamma'_{no}} - \frac{A^+D^+}{\Gamma'_{ni}}\right] \tag{56b}$$

which are expressed here in terms of measured widths Γ'_{no}, Γ'_{ni} and of quanitites such as A^+, B^+, C^+, D^+, ε_2, ε_3, all determined earlier. All the material and geometrical parameters required to completely solve the inverse scattering problem have been determined from the radar reflections.

V. CONCLUSIONS

We have constructed the RST predictions for the reflection coefficient of a bilaminar plane configuration of dielectric layers separating two dissimilar, non-conducting media. This predicition is compared to the classical model prediction. The comparision serves to emphasize the accuracy and simplicity of the Resonance Scattering Theory (8), as well as its ability to yeild a clear physical interpretation of a complex phenomenmom in terms of scattering poles. Furthermore, the RST shows its capability as a material probe to extract geometrical and material composition information from the set of scattering layers returning the reflected radar echoes. This capability is used to completely solve the inverse scattering problem for the bilaminar configuration under analysis. The locations and widths of the resonances as well as their amplitudes determine the thickness and dielectric compositions of both interacting layers. The process disentangles which set of resonance features in the reflected echo is caused by which of the layers. The calculations that we display in many graphs illustrate the case of an oil layer hidden under a covering of ice, both media sandwiched between air on top and water at the bottom. This work could be useful in the further development of techniques for detecting and mapping the extent of an oil spill under solid ice.

ACKNOWLEDGEMENTS

The authors acknowledge the support and encouragement received by the Coast Guard (Dr. C. McKindra, Project Officer) and the Independent Research Board of the Naval Surface Weapons Center (Dr. Pastine, Director).

REFERENCES

1. W. T. Thomson, "Transmission of Elastic Waves Through a Stratified Solid Material". J. Appl. Phys. 21, 89, 1950.

2. W. Weinstein, "The Reflectivity and Transmissivity of Multiple Thin Coatings", J. Optical Soc. Amer. 37, 576, 1946.

3. P. King and L. B. Lockhart, "Two-layered Reflection-Reducing Coatings", J. Optical Soc. Amer. 36, 513, 1946.

4. L. N. Hadley and D. M. Dennison, "Reflection and Transmission Interference Filters", J. Optical Soc. Amer. 37, 451, 1947.

5. P. M. Morse and U. Ingard, Theoretical Acoustics, McGraw-Hill Book Co., New York, N.Y., 1968.

6. L. M. Brekhovskikh, Waves in Layered Media, Academic Press (English translation supervised by R. Bayer), New York, 1960.

7. B. Alder, Editor, Methods in Computational Physics, Academic Press 12, New York, 1972.

8. L. Flax, G. Gaunaurd and H. Überall, "The Resonance Scattering Theory" in Physical Acoustics Vol. 15, Ch. 3, 193-295, Academic Press, N. York, W. P. Mason and R. N. Thurston, Editors, 1981.

9. R. Fiorito and H. Überall, "Resonance Theory of Acoustic Reflection and Transmission Through a Fluid Layer", J. Acoust. Soc. Amer. 65, 9-14, 1979.

10. W. R. Hoover et. al, "Resonances in Acoustic Bottom Reflection and Their Relation to Ocean Bottom Properties", Catholic Univ. of America Report of Jan 14, 1981. (15pp & 7 figs.)

11. G. Gaunaurd et al, "Resonances of Dielectrically-coated Conducting Spheres and the Inverse Scattering Problem", J. Appl. Phys. 52, 35-43, 1981.

12. D. Brill, G. Gaunaurd, and H. Überall, "The Response Surface in Elastic Wave-Scattering", J. Appl. Phys. 52, 3205-3214, 1981.

13. G. Breit and E. Wigner, "Capture of Slow Neutrons", Phys. Rev. 49, 519, 1936.

14. G. Gaunaurd and H. Überall, "R-Matrix Theory of Sound Scattering Via the Mittag-Leffler Expansion", J. Acoust. Soc. Amer. 68, 1850-1857, 1980.

15. G. Gaunaurd and H. Überall, "Numerical Evaluation of Model Resonances in the Echoes of Compressional Waves Scattered from Fluid-filled Spherical Cavities in Solids", J. Appl. Phys. 50, 4342-4660, 1979.

TABLE 1

CASE: Normal Incidence (i.e., $\theta_4 = 0^0$)

LOCATION OF THE RESONANCE FREQUENCIES

	SINGLE LAYER	DOUBLE LAYER		
ℓ	(MHz-meters)	$\alpha = 50{,}000$	$\alpha = 500$	$\alpha = 5$
1	41.9	41.9	41.9	35.2
2	125.8	125.8	125.6	106.4
3	209.6	209.6	209.3	179.2
4	293.5	293.5	292.9	253.1
5	377.3	377.3	376.6	372.2
6	461.2	461.2	460.3	400.5
7	545.0	545.0	544.0	472.2
8	628.9	628.9	627.9	542.7
9	712.8	712.7	711.4	613.5
10	796.6	796.6	795.1	685.7
11	880.5	880.4	878.8	759.4
12	964.3	964.3	962.5	833.6
13	1048.2	1048.1	1046.1	907.2
14	1132.0	1132.0	1129.8	979.4
15	1215.9	1215.8	1213.5	1050.2
16	1299.7	1299.7	1297.2	1120.7
17	1383.6	1383.5	1380.9	1192.4
18	1467.4	1467.4	1464.6	1265.7
19	1551.3	1551.2	1548.3	1339.8
20	1635.1	1635.1	1631.9	1413.7

TABLE 2

CASE: Oblique Incidence at $\theta_4 = 30^0$

LOCATION OF THE RESONANCE FREQUENCIES

	SINGLE LAYER	DOUBLE LAYEP		
ℓ	(MHz-meters)	$\alpha = 50{,}000$	$\alpha = 500$	$\alpha = 5$
1	43.7	43.7	43.6	36.7
2	131.0	131.0	130.7	110.9
3	218.3	218.3	217.9	187.0
4	305.7	305.7	305.1	264.4
5	393.0	393.0	392.2	342.0
6	480.3	480.3	479.4	418.9
7	567.7	567.7	566.6	494.0
8	655.0	655.0	653.7	567.5
9	742.3	742.3	740.9	641.1
10	829.7	829.7	828.1	716.3
11	917.0	917.0	915.2	793.1
12	1004.3	1004.3	1002.4	870.8
13	1091.7	1091.6	1089.6	948.2
14	1179.0	1179.0	1176.7	1024.2
15	1266.3	1266.3	1263.9	1098.5
16	1353.7	1353.6	1351.1	1171.8
17	1441.0	1441.0	1438.2	1246.0
18	1528.3	1528.3	1525.4	1322.1
19	1615.7	1615.6	1612.6	1399.5
20	1703.0	1703.0	1699.8	1477.2

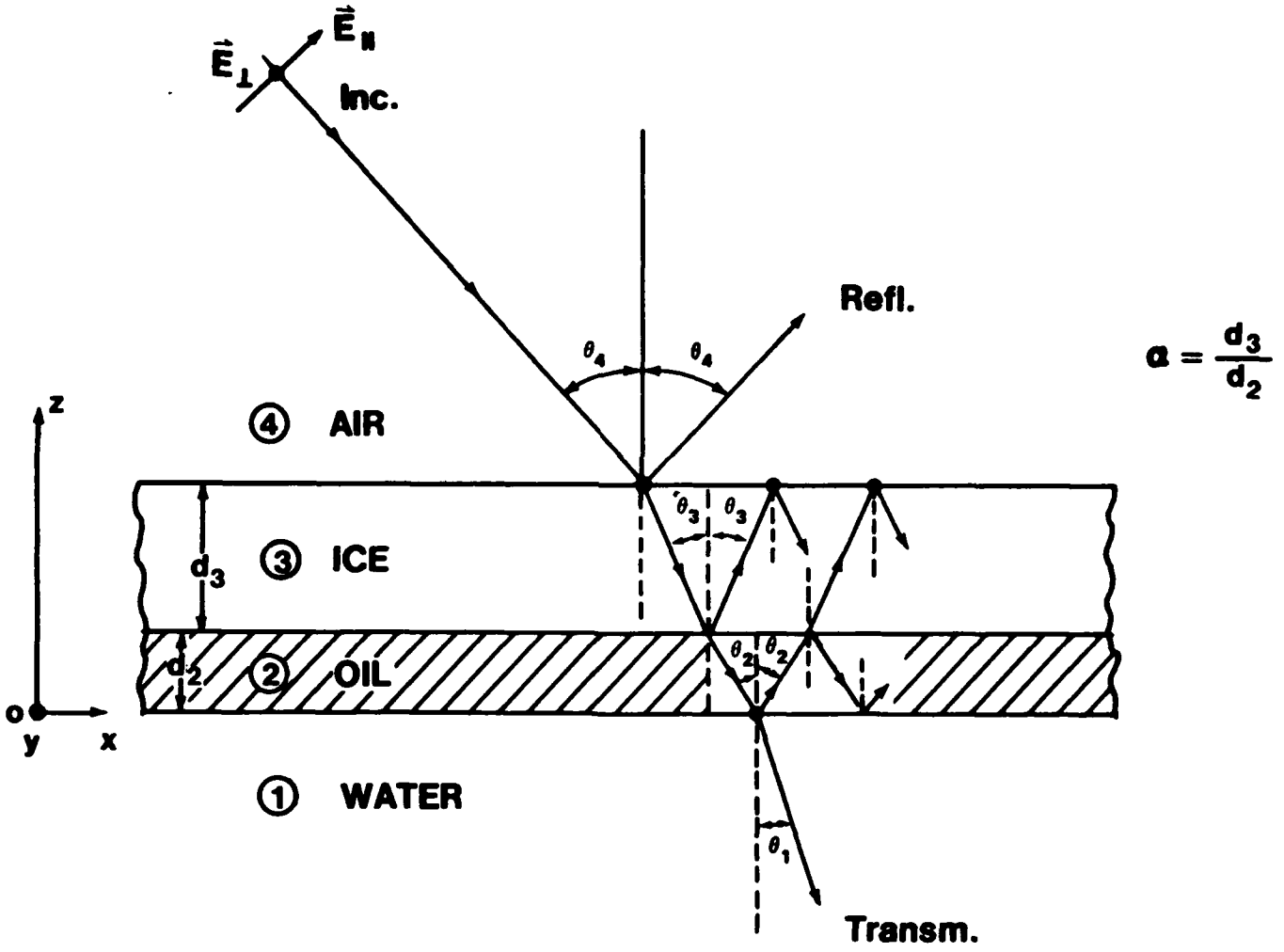

THE GEOMETRY

Fig. 1

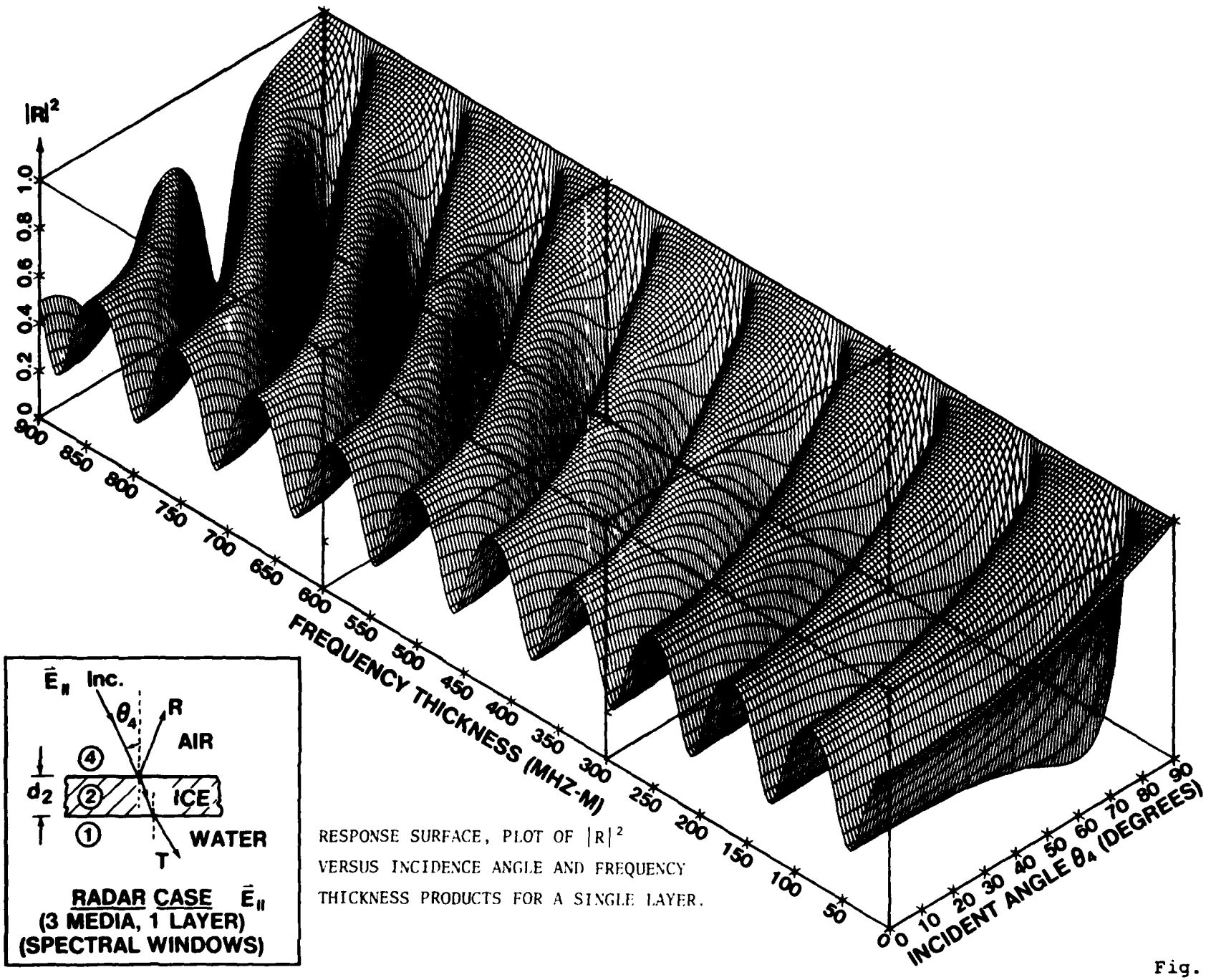

RESPONSE SURFACE, PLOT OF $|R|^2$ VERSUS INCIDENCE ANGLE AND FREQUENCY THICKNESS PRODUCTS FOR A SINGLE LAYER.

Fig. 2

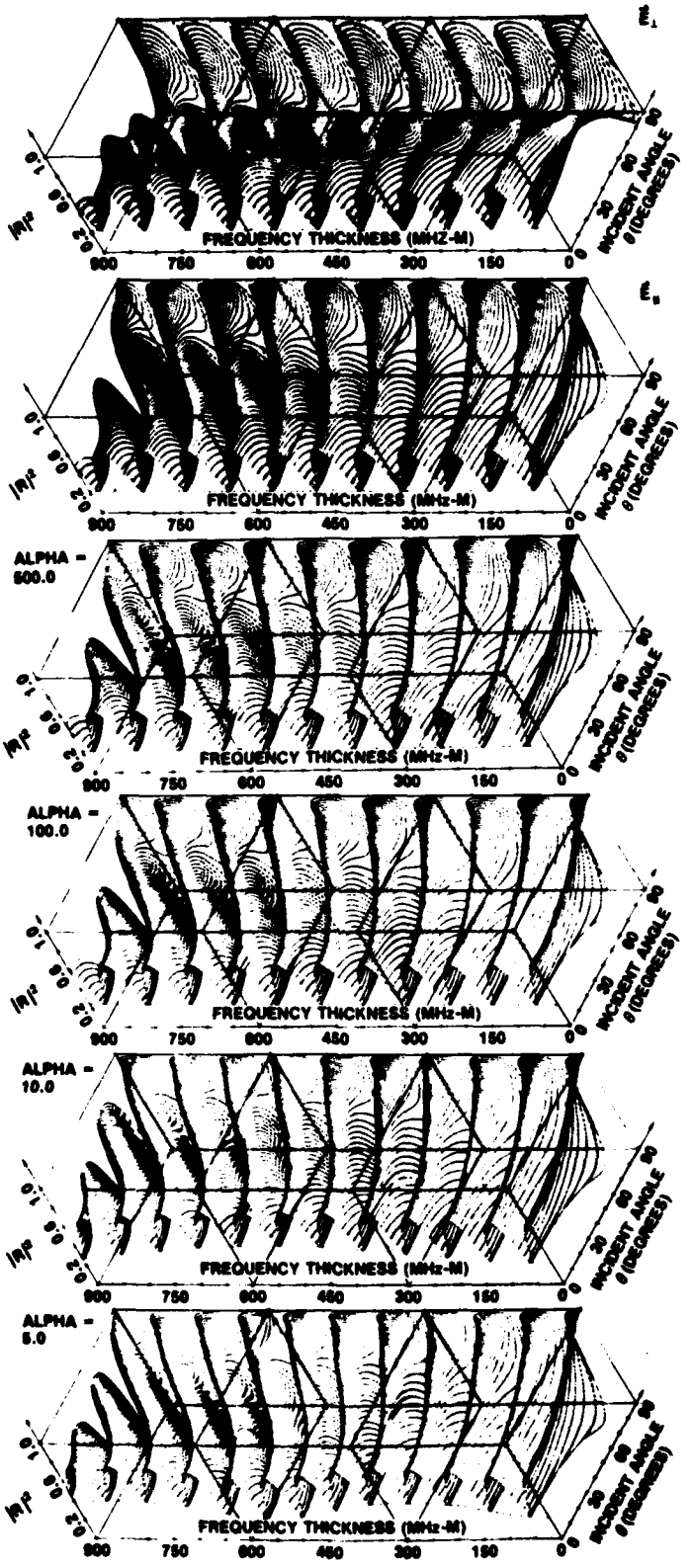

RESPONSE SURFACES FOR SINGLE AND BILAMINAR CONFIGURATIONS

Fig. 3

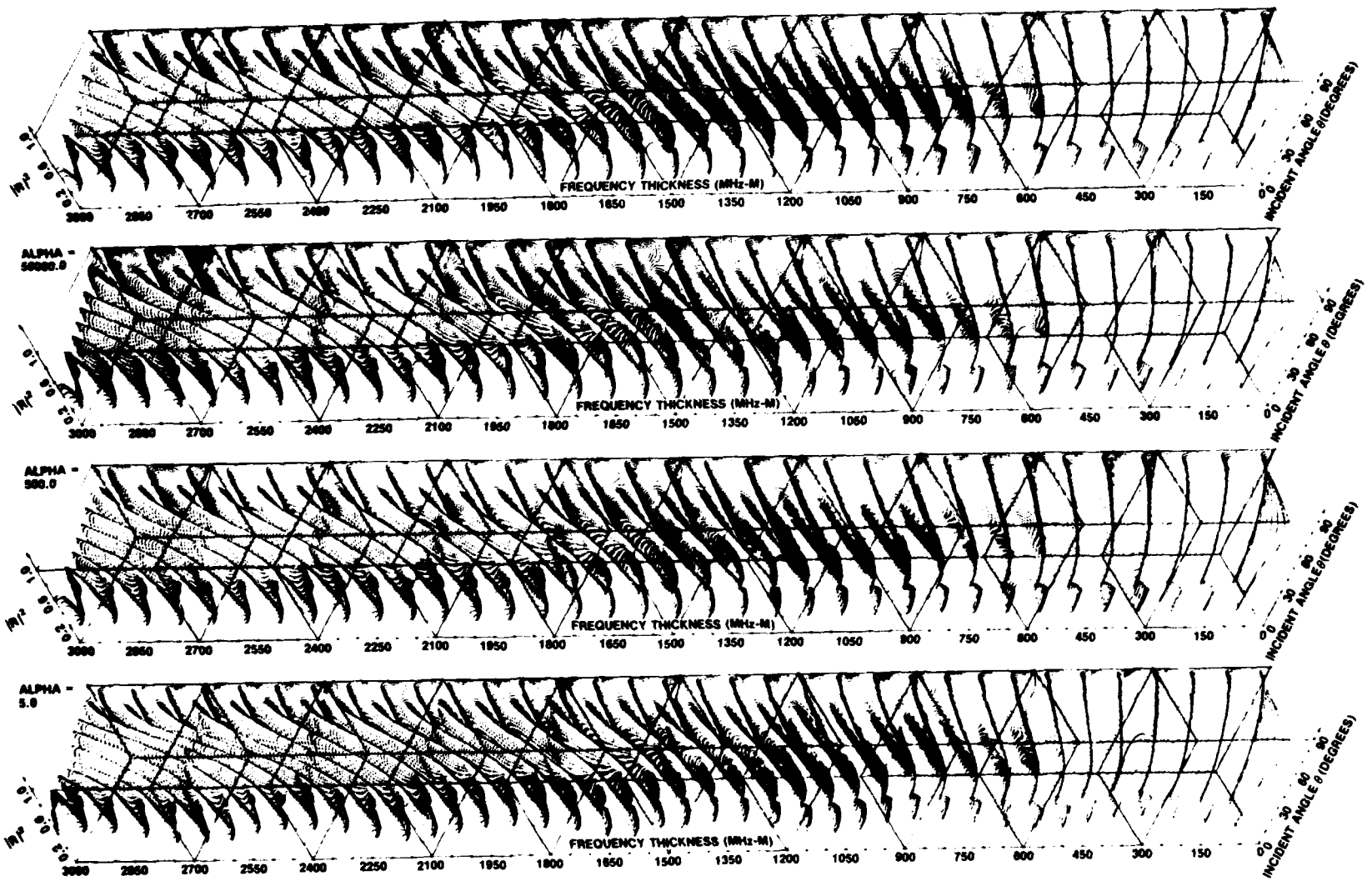

RESPONSE SURFACES FOR SINGLE AND BILAMINAR CONFIGURATIONS FOR FREQUENCY THICKNESS PRODUCTS TO 3000 MHZ-METERS

Fig. 4

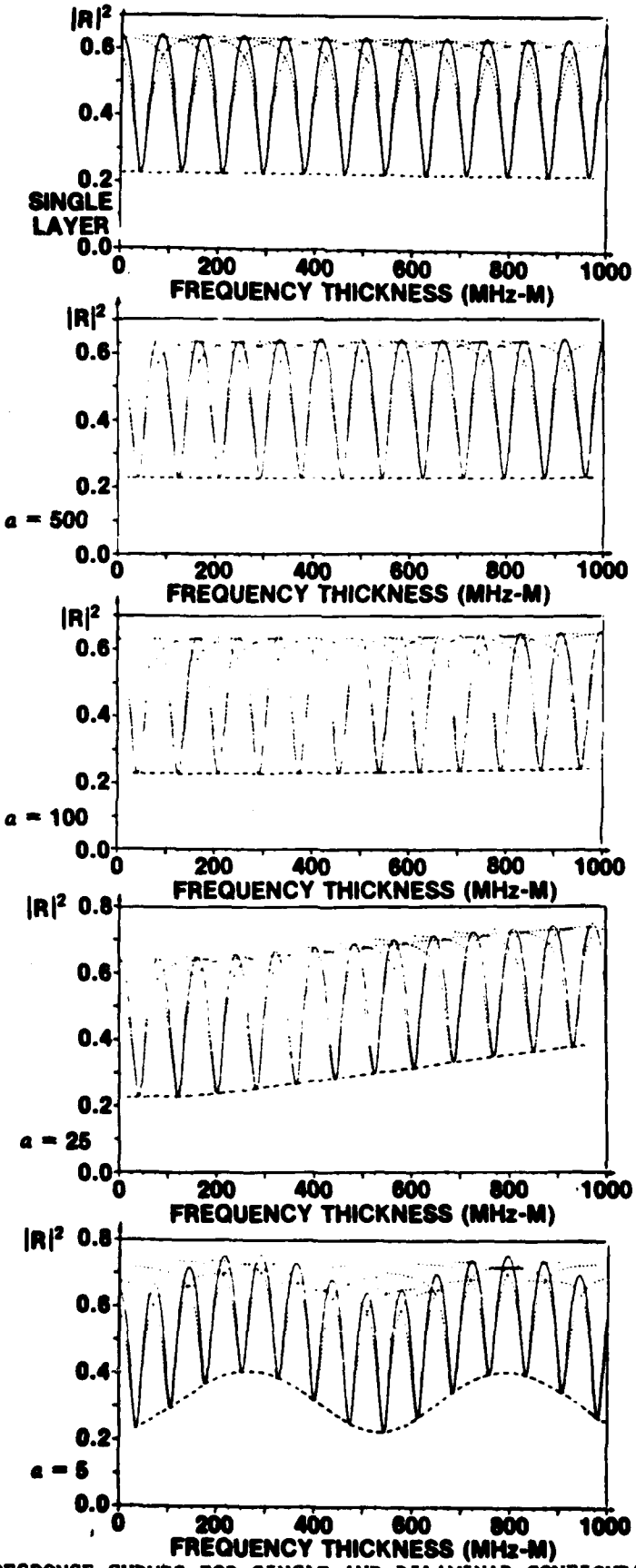

RESPONSE CURVES FOR SINGLE AND BILAMINAR CONFIGURATIONS. SOLID LINE FOR CLASSICAL THEORY, DASHED LINE FOR RST.

Fig. 5

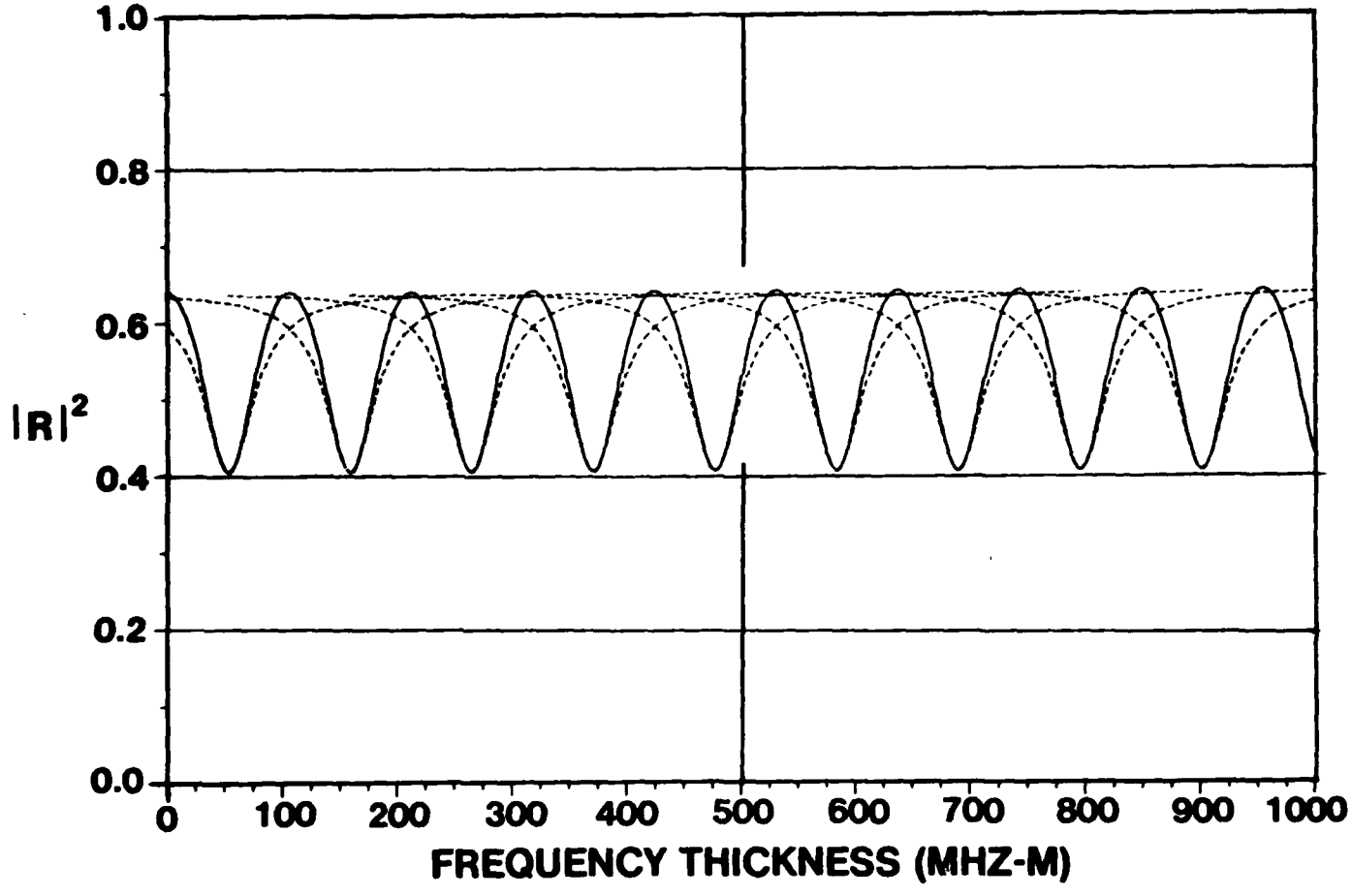

RESPONSE CURVE FOR SINGLE LAYER. SOLID LINE FOR CLASSICAL THEORY, DASHED LINE FOR RST.

Fig. 6